Journal of Solid State Chemistry **168,** 438–443 (2002)
doi:10.1006/jssc.2002.9695

$TTF[Ni(dmit)_2]_2$: Now as Thin Films and Nanowires

Lydie Valade,*[,1] Hélène Casellas,* Stéphane Roques,* Christophe Faulmann,* Dominique de Caro,* Antoine Zwick,† and Lucien Ariès‡

*Equipe "Précurseurs moléculaires et matériaux," CNRS UPR 8241, Laboratoire de Chimie de Coordination, 205 route de Narbonne, 31077 Toulouse Cedex 4, France; †Laboratoire de Physique des Solides, CNRS UMR 5477, 118 route de Narbonne, 31062 Toulouse Cedex 4, France; and ‡Centre Interuniversitaire de Recherche et d'Ingénierie des Matériaux, CNRS UMR 5085, 118 route de Narbonne, 31062 Toulouse Cedex 4, France

Received December 18, 2001; in revised form April 16, 2002; accepted April 26, 2002

Thin films and nanowires of the molecular superconductor $TTF[Ni(dmit)_2]_2$ (TTF = tetrathiafulvalene, $dmit^{2-}$ = 2-thioxo-1,3-dithiol-4,5-dithiolato) are obtained by dipping process on stainless-steel and silicon conversion coatings and on a microrough silicon surface. The deposits are characterized by SEM, Raman spectroscopy and conductivity measurements. © 2002 Elsevier Science (USA)

Key Words: **molecular material; nanowire; thin film; dipping; molecule-based conductor.**

INTRODUCTION

Molecule-based conductors have been known for already 30 years. However, they have been mostly studied as single crystals, though interest in using them in electronic devices has been a permanent goal. The dream may come true if chemical reactions involved in their preparation fit the requirements to be applied to commonly used processing methods such as chemical vapor deposition (CVD), electrochemical coating, sputtering, or dipping process. Previous, non-exhaustive, examples of reports on thin- film preparation of molecule-based materials include the use of Langmuir–Blodgett (1), high vacuum evaporation (2–4), electrochemical deposition (5), molecular beam deposition (6), CVD (7, 8), and reticulate doping (9) techniques. We recently reported the preparation of TTF·TCNQ (TTF = tetrathiafulvalene, TCNQ = tetracyanoquinodimethane) thin films and nanowires using stainless-steel conversion coatings (SSCCs) substrates (10). We could evidence the interest of using such substrates in terms of surface coverage, adhesion, and nanowires growth when performing CVD and dipping process. These results naturally encouraged the study and use of conversion coatings on silicon, the typical microelectronic substrate. Moreover, we expanded the study to another molecule-based conductor: $TTF[Ni(dmit)_2]_2$ (TTF = tetrathiafulvalene, $dmit^{2-}$ = 2-thioxo-1,3-dithiol-4,5-dithiolato) (Fig. 1). This paper will focus on $TTF[Ni(dmit)_2]_2$ thin films and nanowires formation on SSCC, silicon conversion coatings (SiCCs) and microrough silicon (SiMR) substrates using dipping process.

EXPERIMENTAL SECTION

TTF is commercially available. Other starting compounds are prepared following previously described procedures: $(TTF)_3(BF_4)_2$ in (11), the $dmit^{2-}$ ligand in (12), and $[Ni(dmit)_2](NBu_4)$ in (13).

SSCCs preparation follows a controlled oxidation method already described (10, 14). SiCC and SiMR surfaces are prepared by procedures similar to that used for SSCC (15). The arithmetic surface roughness R_a is measured using a TENCOR P2 profilometer. STM studies were run on a Nanoscope II equipment, and SEM on a JEOL model JSM 840A apparatus.

$TTF[Ni(dmit)_2]_2$ thin films and nanowires grow by dipping the SSCC, SiCC or SiMR substrates successively in acetonitrile solutions of $[Ni(dmit)_2](NBu_4)$ ($3.54\,g\,L^{-1}$) and $(TTF)_3(BF_4)_2$ ($2.04\,g\,L^{-1}$). Preparation of the solutions and dipping steps are performed inside an argon-filled

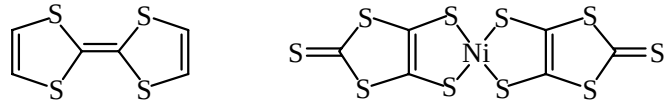

TTF $\qquad$ $Ni(dmit)_2$

FIG. 1. TTF and $Ni(dmit)_2$ molecules. Building blocks of the $TTF[Ni(dmit)_2]_2$ molecular superconductor.

[1] To whom correspondence should be addressed. Fax: +33 05-61-55-30-03. E-mail: valade@lcc-toulouse.fr.

0022-4596/02 $35.00

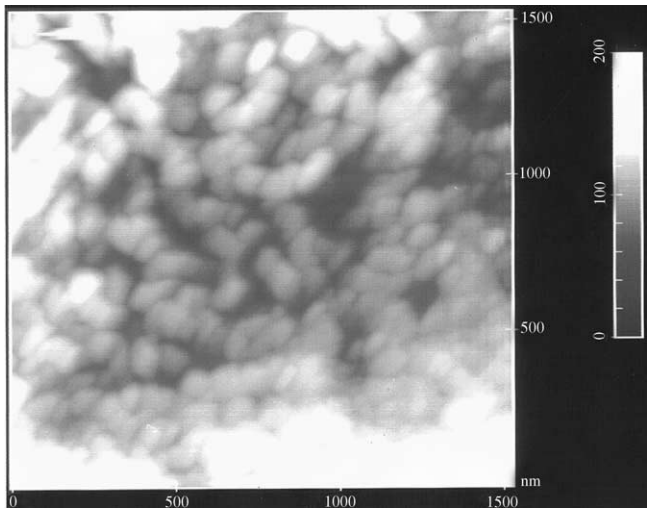

FIG. 2. AFM observation of an SSCC surface.

glove-box. After reaction and drying, the surfaces do not need to be stored under inert atmosphere as TTF[Ni(dmit)$_2$]$_2$ is air stable. The deposits were studied by SEM (JEOL model JSM 840A), Raman spectroscopy (DILOR XY micro-Raman, source: 488 nm line of an Ar laser, laser power density $\approx 10^5\,\mathrm{W\,cm^{-2}}$), and conductivity measurements (home-made equipment, four-probe technique).

RESULTS AND DISCUSSION

Substrates Preparation and Properties

SSCCs grow on austenitic stainless steel-sheets through a combined chemical/electrochemical process. The resulting coatings were identified as magnetite and maghemite phases (16). They have been known for showing advanced adsorption properties due to their fractal-like nanostructured surface (Fig. 2) and were applied to fix dyes (16) or to improve the adherence of further coatings (17). After undergoing the same type of treatment, a silicon wafer surface exhibits similar features (Fig. 3) and consists of nanostructured silicon oxide (SiCC for silicon conversion coating) formed on the honeycomb structure of the non-polished side of the silicon wafer. Through the variation of the conditions of preparation of the SiCC surfaces, we could further isolate oxide-free silicon surfaces (Fig. 4), named microrough silicon (SiMR) as they retain the original microrough morphology of the SiCC (15). A typical roughness profile of the surfaces is shown in Fig. 5 in the case of an SiCC. As a general feature, the R_a values increase by a factor of 2 after chemical treatments of the surfaces.

One can wonder why these modified surfaces exhibit such good adsorption properties? We can see from the above images that the morphology of the surfaces consists of nanopores. In addition to increasing tremendously the overall surface, thus physical adsorption opportunities, these nanopores (SSCC, SiCC and SiMR) act as reservoirs, allowing chemical reactions to take place at a nanoscale

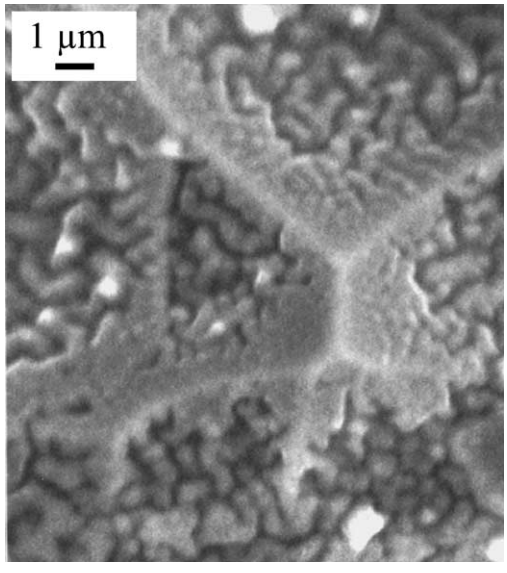

FIG. 3. SEM observation of an SiCC surface.

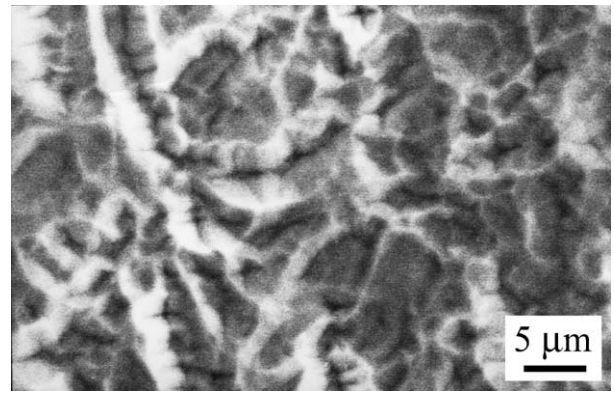

FIG. 4. SEM observation of an SiMR surface.

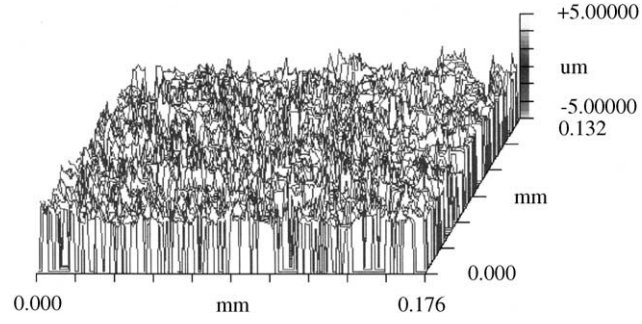

FIG. 5. Typical SiCC surface profile.

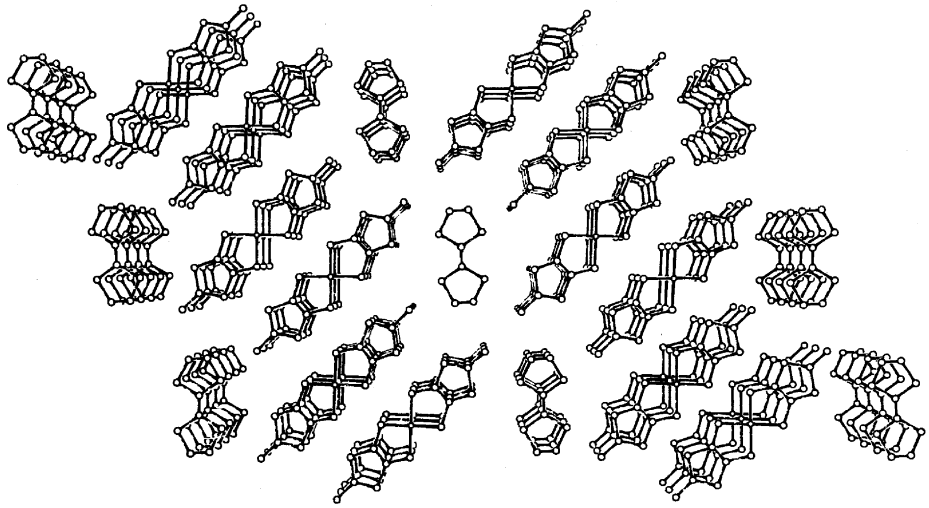

FIG. 6. View of the TTF[Ni(dmit)$_2$]$_2$ structure along the [010] stacking axis.

level. These features are applied here for growing nanowires and films of TTF[Ni(dmit)$_2$]$_2$.

TTF[Ni(dmit)$_2$]$_2$ Deposition

TTF[Ni(dmit)$_2$]$_2$ belongs to the donor–acceptor family of compounds. It results from the reaction of (TTF)$_3$(BF$_4$)$_2$ with [Ni(dmit)$_2$](NBu$_4$) in solution. The reaction leads to the formation of a 1:2 adduct where TTF and [Ni(dmit)$_2$] species are partially oxidized. Within the final material, the charge transfer between the TTF donor molecule and the [Ni(dmit)$_2$] acceptor complex was found to be 0.8 from diffuse X-ray scattering experiments and band structure calculations (18). The structure of TTF[Ni(dmit)$_2$]$_2$ consists of segregated stacks of TTF and [Ni(dmit)$_2$] units (Fig. 6). On single crystal, its room-temperature conductivity is 300 S cm^{-1} at ambient pressure along [010]. The conductivity behavior is metallic down to 4 K. Moreover, this compound undergoes a complete transition to a superconducting state at 1.62 K under a pressure of 7 kbar (19).

When microporous substrates are dipped in a [Ni(dmit)$_2$](NBu$_4$) solution, the nanopores of their surface uniformly adsorb the solution. The adsorbed amount of solution may be increased if the substrate is placed under vacuum before dipping. In a second step, the [Ni(dmit)$_2$](NBu$_4$)-filled surface is dipped in a (TTF)$_3$(BF$_4$)$_2$ solution. At this time, reaction occurs between the two components and TTF[Ni(dmit)$_2$]$_2$ grows on the surface.

Morphology of the TTF[Ni(dmit)$_2$]$_2$ Deposits

Depending on the substrate nature, the deposits exhibit quite different morphologies. On SSCC substrates, SEM images show that the deposits consist of nanowires. The diameter of these nanowires lies from 50 to 150 nm (Fig. 7). Some areas are more covered by nanowires than others. On

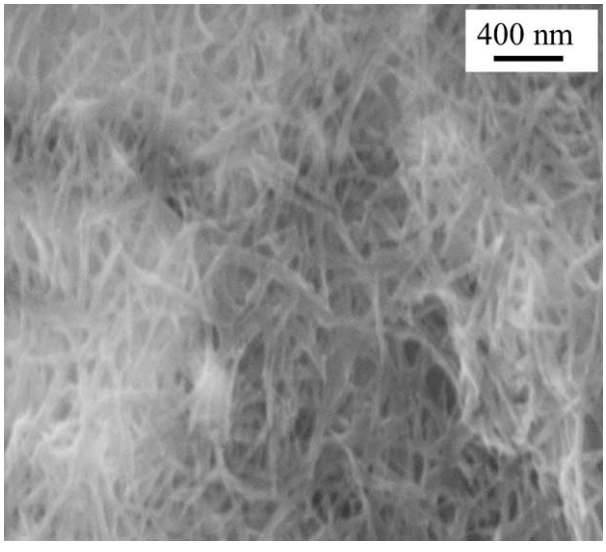

FIG. 7. SEM image of TTF[Ni(dmit)$_2$]$_2$ nanowires on SSCC.

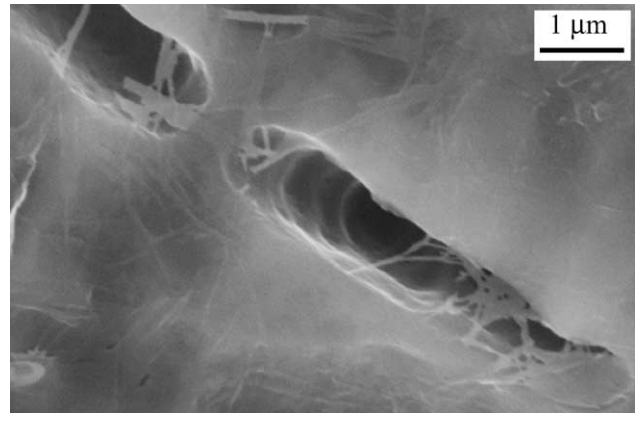

FIG. 8. SEM image of a TTF[Ni(dmit)$_2$]$_2$ film on SiCC.

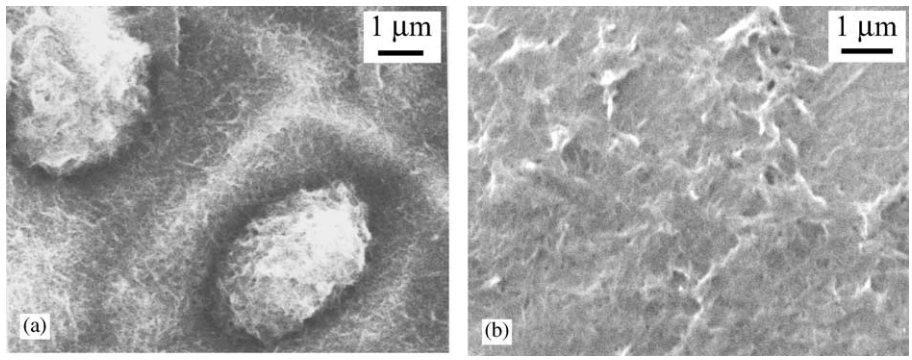

FIG. 9. SEM image of a TTF[Ni(dmit)$_2$]$_2$ deposit on SiMR.

SiCC surfaces, the deposit consists of a thick film (1 μm) (Fig. 8). The film covers all the surface, and is rather dense, though it exhibits a few holes through which nanowires may be observed. When SiMR substrates are used, TTF[Ni(dmit)$_2$]$_2$ fibers fit the morphology of the silicon surface: the holes of the honeycomb silicon structure contain ball-wound fibers (Fig. 9a). Under strong stirring, a more uniform and thicker deposit is obtained (Fig. 9b)

Raman Study of the TTF[Ni(dmit)$_2$]$_2$ Deposits

The Raman spectrum of each deposit was registered and compared to that of the well-identified (TTF)[Ni(dmit)$_2$]$_2$ single crystals. Table 1 gathers the main Raman frequencies for **1** (single crystals), **2** (deposit on SSCC), **3** (deposit on SiCC), and **4** (deposit on SiMR). Raman frequencies for neutral TTF, TTF^+ monocation, neutral Ni(dmit)$_2$, and [Ni(dmit)$_2$]$^-$ monoanion are also summarized in Table 1. The Raman spectrum at HH polarization of (TTF)[Ni(dmit)$_2$]$_2$ single crystals **1** exhibits lines at 256, 757, 1440, 1493, and 1518 cm^{-1}, attributed to the TTF moiety by comparison with Bozio and Pecile (Table 1) (20). The other lines of the Raman spectrum of **1** (332, 355, 495, 1085, and 1320 cm^{-1}) are characteristic of the Ni(dmit)$_2$ moiety (Table 1) (21). The band at 1320 cm^{-1} corresponds to the C=C bonds stretching mode of the nickel bis(dithiolene) fragment. This mode can be evidenced either as a sharp line or as a broad shoulder depending on the crystal face on which the incident laser beam is focused.

Raman spectra of **2**–**4** were recorded at HH polarization after focusing the incident laser beam onto the deposit through the microscope objective, giving a spot size of 1 μm^2. No major degradation of the sample was observed. Raman spectra of the deposits are similar in their general features to that obtained for **1**, as it is shown in Fig. 10. However, the signal-to-noise ratio is lower than that observed for **1**, presumably due to the low amount of deposited material. The $\nu_{C=C}$ stretching mode in Ni(dmit)$_2$ is not observed for **3** and appears as a shoulder in **4**. This could result from a particular orientation of the film onto the substrate surface. The larger observed frequency differences ($\Delta\nu_{obs}$) between neutral and ionized moieties are obtained for C=C stretching vibration modes ($\Delta\nu_{obs} > 50\,cm^{-1}$) (Table 1). In particular, the $\nu_{C=C}$ at

TABLE 1
Raman Shifts of TTF[Nidmit)$_2$]$_2$ Single Crystal 1, Deposits on SSCC 2, on SiCC 3, and on SiMR 4 Compared to Neutral and Ionic Constituting Molecules

	Sample ID							
	1	**2**	**3**	**4**	TTF^0	TTF^+	Ni(dmit)$_2$	[Ni(dmit)$_2$]$^-$
Reference	This work	This work	This work	This work	(20)	(20)	(21)	(21)
δ_{S-C-S} and δ_{C-S-C} in TTF	256	261	255	255	244	265	—	—
$\delta_{out\ of\ plane}$ of five-membered rings in Ni(dmit)$_2$	332	348	342	340	—	—	343	338
ν_{Ni-S} in Ni(dmit)$_2$	355	366	362	364	—	—	364	358
ν_{C-S} of the terminal $S_2C=S$ fragment in Ni(dmit)$_2$	495	501	499	497	—	—	496	507
ν_{C-S} in TTF	757	762	761	755	735	758	—	—
$\nu_{C=S}$ in Ni(dmit)$_2$	1085	1065	1065	1065	—	—	1051	1052
$\nu_{C=C}$ in Ni(dmit)$_2$	1320	1344	Not obs.	1320	—	—	1329	1403
$\nu_{C=C}$ in TTF (central C=C contribution: 71%)	1440	1445	1435	1425	1518	1420	—	—
$\nu_{C=C}$ in TTF (ring C=C contribution: 90%)	1493	1497	1493	1487	1530	1478	—	—
$\nu_{C=C}$ in TTF (ring C=C contribution: 68%)	1518	1527	1522	1517	1555	1505	—	—
Charge transfer ρ	0.77	0.72	0.82	0.90	—	—	—	—

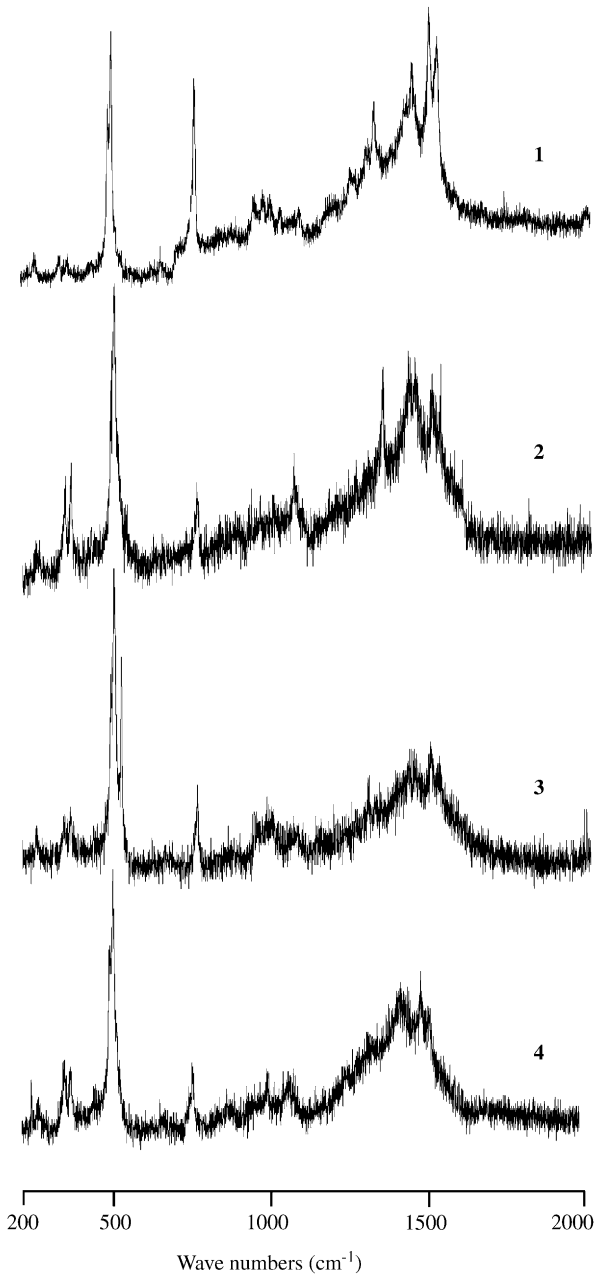

FIG. 10. Raman spectra of $TTF[Ni(dmit)_2]_2$: single crystal 1, deposit on SSCC 2, SiCC 3 and SiMR 4.

$1518\,cm^{-1}$ for neutral TTF ($1420\,cm^{-1}$ for TTF^+), which involves a large contribution of the central carbon–carbon double bond (71%), is very sensitive to the amount of charge transfer (ρ) (22). Furthermore, a linear relationship between this Raman frequency and ρ in a series of partially oxidized TTF salts has been drawn (22). We can thus evaluate the charge transfer from TTF donor to $Ni(dmit)_2$ acceptor for **1–4** (Table 1). Values varying from 0.72 to 0.90 are found. They are in relatively good agreement with that obtained before, i.e., 0.80 (18).

Conductivity Measurement of the $TTF[Ni(dmit)_2]_2$ Deposits

Conductivity measurements could be done on deposits **3** grown as continuous thick films on the SiCC substrates. The standard four-probe technique was used. The conductivity of the film is about $2\,S\,cm^{-1}$. This value is similar to that of powder samples and two orders of magnitude lower than the highest value measured along the needle axis of single crystals ($300\,S\,cm^{-1}$). It agrees with a random contribution of the high intrinsic conductivity of the material and the low conductivity of inter-fiber or inter-grain contacts within the film. Moreover, the films exhibit a pseudo-metallic behavior (Fig. 11) down to low temperature ($R_{4\,K}/R_{300\,K} = 0.8$) which is quite satisfactory for a film and means that the inter-grain contacts do not affect too much the overall electric behavior of the material. The conductivity of the deposit obtained on SiMR under strong stirring is $0.15\,S\,cm^{-1}$ at room temperature. This value is close to that of deposits **3** obtained on SiCC.

CONCLUSION

We have shown that thin films and nanowires of molecular metals may be grown by using a very simple dipping technique in mild conditions. This became possible by the use of a special kind of substrate exhibiting increased adsorption properties due to its peculiar surface morphology. Chemical vapor deposition is not as easy to apply for growing thin films in the case of molecular materials having low volatile precursors. The dipping process is therefore an interesting alternative. Moreover, by varying the growing conditions, nanowires form. This represents an important opening to the use of molecular materials in nanodevices (23). Our present goal is to assemble these nanowires into ordered arrays in order to produce functional systems.

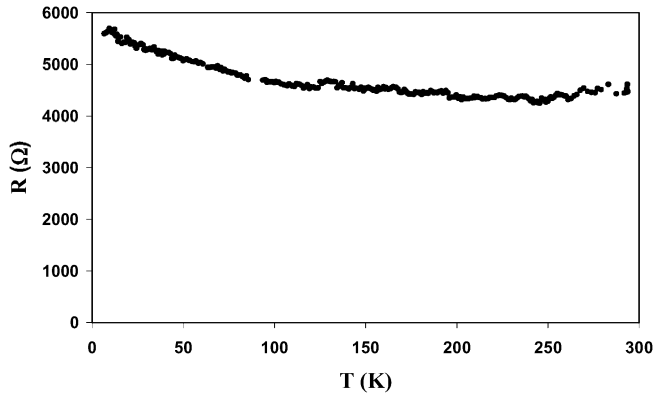

FIG. 11. Resistance of $TTF[Ni(dmit)_2]_2$ films as a function of temperature.

ACKNOWLEDGMENTS

This work was supported by a CNRS NOI program. M. Reversat (ENSIACET) and G. Seine (CEMES) are acknowledged for deposits observations.

REFERENCES

1. H. Li, D. Zhang, Y. Xu, W. Xu, G. Yu, X. Li,D. Zhu, *Synt. Met.* **123,** 385–389 (2001).
2. J. Fraxedas, J. Caro, A. Figueras, P. Gorostiza, and F. Sanz, *J. Vac. Sci. Technol. A* **16,** 2517–2523 (1998).
3. J. Caro, J. Fraxedas, O. Jürgens, J. Santiso, C. Rovira, J. Veciana, and A. Figueras, *Adv. Mater.* **10,** 608–610 (1998).
4. S. Molas, P. Batail, A. Figueras, M. A. Petruska, J. Santiso, D. R. Talham, and J. Fraxedas, *J. Mater. Chem.* **10,** 2662–2665 (2000).
5. A. C. Hillier, J. H. Schott, and M. D. Ward, *Adv. Mater.* **7,** 409–413 (1995).
6. A. Koma, *Prog. Cryst. Growth Charact. Mater.* **30,** 129–152 (1995).
7. M. Deutsch, M. C. Gerstenberg, H. F. Gossenberger, V. S. Ban, and S. R. Forrest, *J. Cryst. Growth* **203,** 412–420 (1999).
8. S. Garelik, J. Vidal-Gancedo, A. Figueras, J. Caro, J. Veciana, C. Rovira, E. Ribera, E. Canadell, and A. Seffar, *Synth. Met.* **76,** 309–312 (1996).
9. E. Laukhina, J. Ulanski, A. Khomenko, S. Pesotskii, V. Tkatchev, L. Atovmyan, E. Yagubskii, C. Rovira, J. Veciana, J. Vidal-Gancedo, and V. Laukhin, *J. Phys. I France* **7,** 1665–1675 (1997).
10. D. de Caro, J. Sakah, M. Basso-Bert, C. Faulmann, J.-P. Legros, T. Ondarçuhu, C. Joachim, L. Ariès, L. Valade, and P. Cassoux, *C. R. Acad. Sci. Paris Sér. IIc* **3,** 675–680 (2000).
11. F. Wudl, *J. Amer. Chem. Soc.* **97,** 1962–1964 (1975).
12. L. Valade, J.-P. Legros, M. Bousseau, P. Cassoux, M. Garbauskas, and L. V. Interrante, *J. Chem. Soc. Dalton Trans.* 783–794 (1985).
13. G. Steimecke, H.-J. Sieler, R. Kirmse, and E. Hoyer, *Phosphorus Sulfur* **7,** 49–55 (1979).
14. L. Ariès, J. Roy, T. Bouissou, and R. Sempere, *Mat. Sci. Technol.* **7,** 24–27 (1991).
15. D. de Caro, L. Valade, and L. Ariès, unpublished results.
16. L. Ariès and J.-P. Traverse, European Patent, Europe, 87 4000 318, 1987.
17. L. Ariès, *J. Appl. Electrochem.* **24,** 554–558 (1994).
18. P. Cassoux and L. Valade, *in* "Inorganic Materials" (D. W. Bruce and D. O'Hare, Eds.), pp. 1–64. J. Wiley & Sons, Chichester, 1996.
19. L. Brossard, M. Ribault, M. Bousseau, L. Valade, and P. Cassoux, *C. R. Acad. Sci. Paris* **302-II,** 205–210 (1986).
20. R. Bozio and C. Pecile, *in* "The Physics and Chemistry of Low Dimensional Solids" (L. Alcácer, Ed.), pp. 165–186. D. Reidel Publishing Company, Dordrecht, 1980.
21. K. I. Pokhodnya, C. Faulmann, I. Malfant, R. Andreu-Solano, P. Cassoux, A. Mlayah, D. Smirnov, and J. Leotin, *Synth. Met.* **103,** 2016–2019 (1999).
22. A. R. Siedle, *in* "Extended Linear Chain Compounds" (J. S. Miller, Ed.), Vol. 2, pp. 469–487. Plenum Press, New York, 1982.
23. C. N. R. Rao and A. K. Cheetham, *J. Mater. Chem.* **11,** 2887–2894 (2001).